Toward Tailored Rehabilitation by Implementation of a Novel Musculoskeletal Finite Element Analysis Pipeline

Amir Esrafilian, Lauri Stenroth, Mika E. Mononen, Paavo Vartiainen, Petri Tanska, Pasi A. Karjalainen, Juha-Sampo Suomalainen, Jari P. A. Arokoski, David J. Saxby, David G. Lloyd, and Rami K. Korhonen

***Abstract*— Tissue-level mechanics (e.g., stress and strain) are important factors governing tissue remodeling and development of knee osteoarthritis (KOA), and hence, the success of physical rehabilitation. To date, no clinically feasible analysis toolbox has been introduced and used to inform clinical decision making with subject-specific in-depth joint mechanics of different activities. Herein, we utilized a rapid state-of-the-art electromyography-assisted musculoskeletal finite element analysis toolbox with fibril-reinforced poro(visco)elastic cartilages and menisci to investigate knee mechanics in different activities. Tissue mechanical responses, believed to govern collagen damage, cell death, and fixed charge density loss of proteoglycans, were characterized within 15 patients with KOA while various daily activities and rehabilitation exercises were performed. Results showed more inter-participant variation in joint mechanics during rehabilitation exercises compared to daily activities. Accordingly, the devised workflow may be used for designing subject-specific rehabilitation protocols. Further, results showed the potential to tailor rehabilitation exercises, or assess capacity for daily activity modifications, to optimally load knee tissue, especially when mechanically-induced cartilage degeneration and adaptation are of interest.**

***Index Terms*— Knee osteoarthritis, electromyography assisted musculoskeletal modeling, clinical assessment, rehabilitation exercises, daily activities.**

Manuscript received June 4, 2021; revised October 7, 2021, January 10, 2022, and March 5, 2022; accepted March 7, 2022. Date of publication March 14, 2022; date of current version March 30, 2022. This work was supported in part by the National Health and Medical Research Council of Australia under Grant 2001734; in part by the European Union's Horizon 2020 Research and Innovation Program under the Marie Sklodowska-Curie Grant 713645; in part by the Academy of Finland under Grant 324529, Grant 324994, Grant 328920, Grant 332915, and Grant 334773 (under the frame of ERA PerMed); in part by the Sigrid Juselius Foundation; in part by the Business Finland under Grant 3455/31/2019; in part by the Finnish Cultural Foundation under Grant 191044 and Grant 200059; in part by the Päivikki and Sakari Sohlberg Foundation; in part by the Innovation Fund Denmark under Grant 9088-00006B (under the frame of ERA PerMed); in part by the European Regional Development Fund (Regional Council of Pohjois-Savo) and the University of Eastern Finland under Projects: Human measurement and analysis—research and innovation laboratories under Project A73200 and Project A73241; and in part by the Digital Technology RDI Environment under Project A74338. *(Corresponding author: Amir Esrafilian.)*

This work involved human subjects or animals in its research. Approval of all ethical and experimental procedures and protocols was granted by the Northern Savo Hospital District Ethics Committee under Permission No. 750/2018.

Amir Esrafilian, Mika E. Mononen, Paavo Vartiainen, Petri Tanska, Pasi A. Karjalainen, and Rami K. Korhonen are with the Department of Applied Physics, University of Eastern Finland, 70210 Kuopio, Finland (e-mail: amir.esrafilian@uef.fi).

Lauri Stenroth is with the Department of Applied Physics, University of Eastern Finland, 70210 Kuopio, Finland, and also with the Department of Biomedical Sciences, University of Copenhagen, 1165 Copenhagen, Denmark.

Juha-Sampo Suomalainen is with the Department of Clinical Radiology, Kuopio University Hospital, 70210 Kuopio, Finland.

Jari P. A. Arokoski is with the Department of Physical and Rehabilitation Medicine, Helsinki University Hospital, 00280 Helsinki, Finland, and also with the Department of Surgery, University of Helsinki, 00100 Helsinki, Finland.

David J. Saxby and David G. Lloyd are with the Griffith Centre of Biomedical and Rehabilitation Engineering (GCORE), Menzies Health Institute, Queensland and Advanced Design and Prototyping Technologies Institute (ADAPT), and the School of Health Sciences and Social Work, Griffith University, Gold Coast, QLD 4222, Australia.

This article has supplementary downloadable material available at https://doi.org/10.1109/TNSRE.2022.3159685, provided by the authors.

Digital Object Identifier 10.1109/TNSRE.2022.3159685

I. Introduction

KNEE osteoarthritis (KOA) is a degenerative joint disease causing pain and inducing functional disabilities with an estimated lifetime risk of ∼14% [1]. Joint tissue mechanics during different motor tasks are altered by the individual's muscle recruitment strategy, muscle strengths, and movement patterns, all of which may contribute to the development of KOA [2]–[5]. Furthermore, the success of different knee surgeries (e.g., anterior cruciate ligament reconstruction) depends on the post-surgery joint loading regulated through physical rehabilitation [6]–[8]. Rehabilitation exercises aim to strengthen muscles surrounding the knee, manipulate local joint loading, reduce symptoms of pain, swelling, and dysfunction [7]–[10]. However, rehabilitation protocols have been developed based on clinical experience and are typically with a one-size-fits-all approach, lacking an in-depth knowledge of localized joint loading gathered from experiments and/or simulations [7]–[9], [11], [12]. As a result, poor clinical outcomes from rehabilitation protocols and interventions are common [13]–[17].

Joint contact forces (JCF) and contact pressures in several functional activities have been measured experimentally; however, those measurements are limited to specific subjects (i.e., those with instrumented implants) [18], [19] or require highly invasive methods [20]. More importantly, these measurements provide no information on tissue-level joint mechanics gov-

This work is licensed under a Creative Commons Attribution 4.0 License. For more information, see https://creativecommons.org/licenses/by/4.0/

erning the onset and progression of musculoskeletal (MS) disorders such as KOA. Alternatively, MS finite element (MS-FE) models, which are low cost and non-invasive, have been developed to estimate tissue mechanics [21]–[23] and predict adaptation and degeneration of knee cartilages and menisci [24]–[26].

Physiological soft-tissue material models (i.e., utilized in the MS-FE models) can influence estimated tissue mechanics in different ways. Specifically, a fibril-reinforced poro(visco)elastic (FRPVE) material model is essential to estimate time-dependent mechanical responses of both fibrillar (collagen) and nonfibrillar (proteoglycans) matrices within, for example, knee cartilages and menisci [25]–[27]. The constitutive formulation of fibril-reinforced material models originates from the main components of articular soft tissues (collagens, proteoglycans, and fluid), and can distinguish the contribution of each tissue component to the overall tissue mechanics. Importantly, mechanical responses of fibrillar and nonfibrillar matrices are believed to have a major involvement in cartilage degeneration, e.g., by replicating the tissue's collagen network damage, cell death, and fixed charged density loss of proteoglycans [24]–[26]. Despite the wealth of mechanistic insight provided by models with FRPVE material and subject-specific joint geometries, creating these models and then conducting the analysis typically takes several weeks/months and requires advanced expertise [28]. Hence, these complex and promising models are strictly limited to research studies with a small number of participants and are impractical for clinical use.

Nevertheless, remarkable efforts are made to develop knee joint MS-FE models capable of incorporating a 12 degrees of freedom (DoFs) knee joint [21], [23], [29]–[33], complex soft tissue material models [21], [34], [35], and subject's muscle activation patterns (EMG-assistance) [36], [37]. However, previous studies have investigated only healthy subjects [21], [34], [38], used simplified joint models in terms of limited DoFs [9], [39], did not include subject-specific joint geometries [9], [38], [39] and muscle activation patterns [22], [23], [32], [34], [38]–[40], neglected crucial joint tissues such as menisci [9], [38], and/or employed simplistic soft tissue material models [31], [38]. To the best of our knowledge, there are no studies that have included the aforementioned complex FRPVE soft-tissue material model in the MS-FE framework to characterize detailed knee cartilage mechanics in different functional activities other than walking gait. Importantly, using subject-specific joint geometries and multi DoFs joint models [23], [41], incorporating subject's muscle activation pattern, including menisci [42], and employing physiological tissue material models will substantially alter estimated tissue mechanics [27], [43]–[45] and our understanding of the effects of motor tasks on tissue mechanics.

Here in the current study, we aimed to evaluate the mechanical responses of knee cartilages and menisci, particularly those related to the fibrillar (collagen) and nonfibrillar (proteoglycans) matrices, of individuals with KOA while they performed different daily activities and rehabilitation exercises. For this aim, we utilized a previously developed semi-automatic atlas-based MS-FE modeling pipeline [36], considering subject-specific muscle activation patterns and the FRP(V)E material model of cartilages and menisci. We hypothesized that the novel EMG-assisted MS-FE modeling method would show highly personalized mechanical responses of cartilage, indicative of tissue health and degeneration, in different functional activities. This will evidence the need to tailor rehabilitation protocols for individuals with KOA to optimize tissue-level responses.

II. Methods

A. Data Collection and Pre-Processing

Fifteen subjects (9 females and 6 males, 62.4±7.8 years old, with body mass index 29.3±6.8 kg/m^2) participated in this study (workflow in Fig. 1). Detailed participant characteristics are provided in supplementary data 1 (Table S.1.1). Inclusion criteria were previously diagnosed KOA evidenced by radiographic joint tissue deterioration and knee pain [46] in at least one or more of the medial or lateral femur, tibia, or patella articular surfaces. Exclusion criteria were the presence of pain in any body parts except for the knee or any record of lower limb surgeries or diagnosed disorders such as ligament or tendon rupture. An expert clinician supervised the subject recruitment process, with the most affected leg of each subject (in terms of KOA severity and pain) selected for analysis (15 knees, one knee from each subject). All procedures were approved by the Northern Savo Hospital District ethics committee (permission No. 750/2018) and written informed consent was obtained from each participant.

Seven daily activities and seven rehabilitation exercises were analyzed in this study (supplementary data 1, Fig. S.1.1). Daily activities consisted of (1) chair stand-to-sit, (2) chair sit-to-stand, (3) walking gait at a habitual speed (1.34±0.14 m/s), (4) walking gait at a preselected constant speed (1.20±0.05 m/s), (5) picking up a light object (a pen) from the ground, (6) stair descent, and (7) stair ascent. Rehabilitation exercises, chosen from a previous study [47], consisted of (1) balance, (2) chair up and down, (3) forward-backward stepping, (4) knee extension with elastic band resistance, (5) side slide exercise, (6) steps up and down, and (7) forward-backward touch down. These exercises have been designed to load the quadriceps muscles and improve control of knee motion and posture [47]. Participants first performed the daily activities in their preferred manner, and then the rehabilitation exercises focusing on loading and seeking good muscular control of their most affected leg, as instructed by the rehabilitation protocols [47]. All daily activities and rehabilitation exercises were performed in a random order, and five successful trials per task for each participant were selected for analyses (i.e., trials without technical issues such as EMG artifacts and missed markers, foot on the edge of the force plate, etc.).

Motion data consisting of 3-dimensional (3D) marker trajectories (100 Hz, Vicon, UK) were synchronously recorded with ground reaction forces (two force plates, 1000 Hz, OR6-7MA, AMTI, USA), and EMGs (1000 Hz, ME6000, Bittium Biosignals Ltd, Finland). EMGs from 8 muscles of the studied leg, consisting of the vastus medialis and lateralis, rectus femoris, medial and lateral gastrocnemius, biceps femoris, semitendinosus and gluteus medius, were recorded according to the SENIAM instructions [48]. Magnetic resonance imaging (MRI) was performed on the most affected knee of each

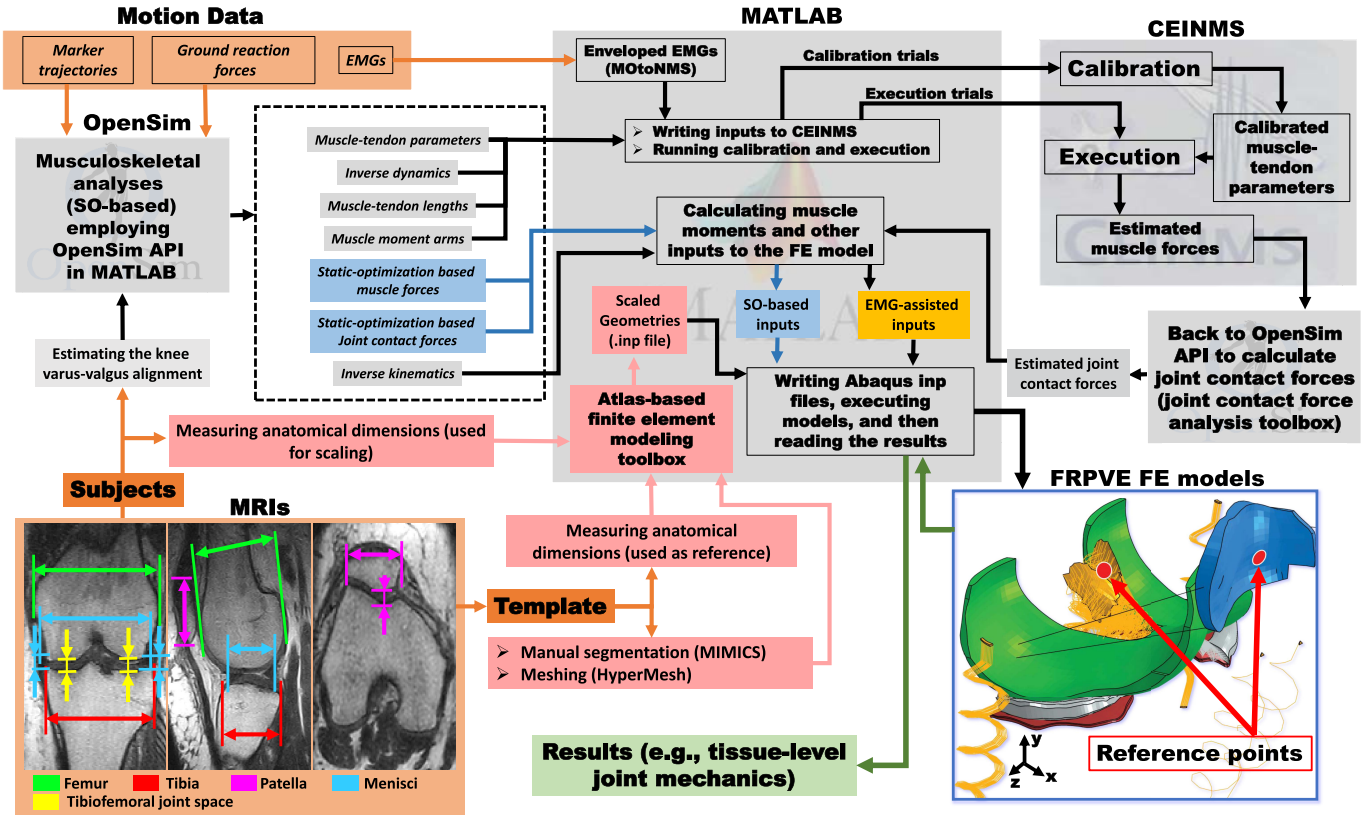

Fig. 1. The workflow of the study: the rapid EMG-assisted musculoskeletal finite element modeling and analysis pipeline. Orange shows inputs to the pipeline, pink shows atlas-based finite element modeling toolbox, blue shows the static-optimization-based workflow, and green shows examples of estimated subject-specific tissue-level joint mechanics.

participant using a 0.18T scanner (Esaote E-Scan XQ, Esaote, Genoa, Italy) consisted of 3D CE sequence (0.89 mm slice thickness, 0.625 mm in-plane resolution). The 3D CE sequence from the 0.18T scanner has earlier been shown to result in adequate knee segmentations with a similar volume and thickness, compared to a 3T scanner (Philips, Best, Netherlands) [40]. A musculoskeletal radiologist performed clinical evaluations of the MRI's upon which abnormalities and cartilage defects were diagnosed (supplementary data 1, Fig. S.1.2). Detailed explanations regarding the activities, data collection, and data processing are provided in supplementary data 1.

B. Musculoskeletal Analyses

To investigate the influence of incorporating the subject's muscle recruitment strategy within the analyses, we compared different joint-level and tissue-level results between the EMG-assisted MS-FE workflow and those from a conventional static optimization (SO) based MS-FE workflow. For both workflows, we used the same dataset. This investigation was needed because, compared to the EMG-assisted MS modeling, the SO-based approach is faster and needs considerably less effort in acquiring data and analysis, but producing results that may not be physiologically plausible [49]. Implementation of the EMG-assisted and SO-based workflows is described below but results and discussion of the SO-based analyses are provided only in supplementary data 1 to 4.

1) The MS Model and Inputs to the MS Analyses: EMG-assisted and SO-based MS analyses used an MS model that included a knee joint with 1 primary DoF, i.e., knee flexion, optimized to enable analysis of motor activities involving deep knee and hip flexions [50]. Additional to flexion, the knee joint had extra DoFs to be able to calculate the associated joint moments and muscle moment arms, but did not influence the inverse kinematics and dynamics solutions (i.e., non-contributing). However, since marker-based motion analysis are reported to be inaccurate in estimating knee secondary kinematics during dynamic activities [51], the knee's extra DoFs for all the MS models were either locked (e.g., abduction/adduction and internal/external rotations) or defined as a function of the knee flexion angle (e.g., tibiofemoral translations and patella DoFs) [50], [52]. Importantly, previous studies, including ours on the development of the current workflow [21], [36], [37], [53], have shown that a 12 DoFs FE knee model driven by a 1 DoF knee EMG-assisted MS model is capable of estimating knee joint kinetics, secondary kinematics, and tissue mechanics consistent with in vivo data and those of a similar FE model when driven by a 12 DoFs knee MS model. Likewise, it has been reported that muscle activation patterns, as used in the current study to inform the MS analyses, are directed to effectively stabilize knee abduction/adduction moment and well estimate JCFs even when using an MS model with a 1 DoF knee joint [54].

Using OpenSim (v 4.1) [55], body segments and length-dependent muscle properties of the MS model were linearly scaled for each participant, using their body mass and length of the limbs from a static trial of upright double support standing. During this process, the tibiofemoral abduction/adduction DoF

was opened to allow the adduction/adduction angle to be adjusted to the individual [56]. The knee alignment estimated by this approach has been reported to be correlated with that measured from frontal plane radiographs of the entire lower extremity during double support standing [57]. Accounting for the inter-individual differences in knee abduction/adduction alignment in KOA patients [58] may improve the estimation of the activation level of knee crossing muscles [59], [60]. Finally, maximum isometric muscle forces of the MS models were scaled by the ratio of the subject's mass to the mass of the unscaled model. After scaling the models, knee abduction/adduction DoF was locked to the calculated value for the rest of the MS analysis.

The OpenSim application programming interface (API) for MATLAB gives access to the functions and capabilities of the OpenSim software within MATLAB m-files to create and update MS models and execute different OpenSim toolboxes and analyses modules. Hence, the OpenSim API for MATLAB and scaled models (i.e., 15 MS models in total) were used to execute inverse kinematics, inverse dynamics (to calculate knee external moments), and SO-based muscle force estimation. Then muscle moment arms, muscle-tendon lengths, and tibiofemoral and patellofemoral JCFs were calculated using OpenSim analysis toolbox via the API (i.e., muscle analysis and joint reaction tools, respectively) [36]. Muscle-tendon moment arms and muscle-tendon lengths were calculated to be used as input to the EMG-assisted MS model (section II.B.2), and later to calculate the corresponding inputs for the FE models of the study (section II.C.2) (Fig.1). The muscle moment arms were extracted for flexion/extension, abduction/adduction, and internal/external DoFs of both the tibiofemoral and patellofemoral joints [36]. For the sake of clarity, we note that in this manuscript, JCF in the MS analysis refers to the joint reaction force reported by the OpenSim joint reaction analysis tool [61].

2) The EMG-Assisted and SO-Based MS Analyses: The EMG-assisted MS analysis of the study was performed using the Calibrated EMG-Informed Neuromusculoskeletal Modelling Toolbox (CEINMS) [21], [36], [62]. Inputs to the CEINMS consisted of (1) muscle-tendon properties, (2) EMG envelopes, (3) joint external moments of the test leg, (4) muscle-tendon moment arms, and (5) muscle-tendon lengths. Muscle-tendon properties of all the 40 muscles of the leg of interest were imported into the CEINMS, including maximum isometric force, tendon slack-length, optimal fiber length, and pennation angle, which were obtained from the MS models (section II.B.1), separately for each subject.

A multi-DoFs calibration for each subject [36], [63] was performed within the CEINMS to optimize the neuromuscular parameters of all the muscles of the study leg [64], [65]. Five DoFs calibration was undertaken, consisting of rotations about the hip (3 DoFs), knee (1 DoF), and ankle (1 DoF). Following calibration, the hybrid mode of the CEINMS toolbox, which included elastic tendons with muscle activation and contraction dynamics, was used to perform the EMG-assisted MS analyses (Fig. 1). More information on the calibration and execution of the EMG-assisted MS analyses are provided in supplementary data 1.

The SO-based muscle forces were estimated (within the OpenSim SO toolbox) to track the joint external moments while minimizing the sum of squared muscle activations. Rigid tendons were used, while muscle activation dynamics (i.e., the relationship between excitation and activation of a muscle) could not be included in SO-based MS analyses due to limitations in OpenSim. However, the muscle contraction dynamics [66] (i.e., the force-length-velocity relationship of muscles) were included.

Finally, the muscle forces estimated by both EMG-assisted and SO-based MS analyses were used to provide the FE models with 2 separate sets of boundary condition and loading inputs, i.e., EMG-assisted and SO-based inputs (see Fig. 1 and section II.C.2: loading and boundary conditions).

C. FE Analyses Workflow

1) Joint Geometries and Material Models (i.e., the Atlas-Based FE Modeling Toolbox): A previously developed and validated atlas-based MS-FE modeling toolbox [36], [67] was exploited to create the FE models (Fig. 1). The knee joint template was from our previous study [36] and consisted of femoral, tibial, and patellar cartilage, menisci, anterior and posterior cruciate ligaments (ACL and PCL), medial and lateral collateral ligaments (MCL and LCL), medial and lateral patellofemoral ligaments (MPFL and LPFL), and patella tendon (Fig. 1). The template was anisotropically scaled according to the morphological dimensions measured separately from each participant's MRI (Figs. 1 and S.1.3). The measurements (explained in more detail later in this section) consisted of mediolateral, anteroposterior, and transverse dimensions, as well as the thickness of femoral, tibial, and patellar cartilages, and menisci (Figs. 1 and S.1.3) [36]. Participants had no records of knee surgeries, ligaments and meniscal injuries, and total cartilage loss or lesions. Insertion points on each end of the ligaments were scaled according to the corresponding morphological dimensions of the femur, tibia, and patella [36]. An MS radiologist supervised the morphological measurements to ensure consistent measurements for different participants.

In the frontal plane (Figs. 1 and S.1.3), first, the image slice with the maximum width of femoral condyles was selected. Then from the selected image, widths and thicknesses of femoral and tibial cartilages and menisci, as well as the outer edge (distance) of the medial and lateral menisci, were measured. In the sagittal plane (Figs. 1 and S.1.3), first, the image slices with the maximum anterior-posterior length of the femoral cartilage were selected separately for medial and lateral femoral condyles. Then anteroposterior dimensions of the femoral and tibial cartilages and menisci (i.e., the outer edges of medial and lateral meniscus) were measured separately for medial and lateral sides (Fig. S.1.3). Patellar cartilage dimensions (i.e., thickness, width, and height) were measured from the image slice with the maximum width of the patella (in the transverse plane, Figs. 1 and S.1.3) or the slice from the femoral groove (sagittal plane. Figs. 1 and S.1.3), correspondingly.

Femoral, tibial, and patellar cartilages were modeled as fibril-reinforced poroviscoelastic (FRPVE) material [68]–[74],

and menisci were modeled as fibril-reinforced poroelastic (FRPE) [75] material. Knee ligaments (i.e., ACL, PCL, MCL, LCL, MPFL, and LPFL), patella tendon, and menisci horn attachments were modeled using spring bundles [76]–[79]. Details of the template scaling and material models are provided in supplementary data 1.

2) Loading and Boundary Conditions: We employed our previously developed muscle-force driven FE modeling approach [36], [67], such that boundary condition and loading inputs to the FE models of the current study consisted of 1) knee flexion angle, 2) knee external abduction/adduction and internal/external moments around the tibiofemoral joint center (determined by inverse dynamics), 3) abduction/adduction and internal/external moments generated by the muscles around the tibiofemoral joint center, 4) flexion/extension, abduction/adduction, and internal/external moments generated by the quadriceps muscles around the patellofemoral joint center, 5) tibiofemoral JCFs, and 6) patellofemoral JCFs (supplementary data 3). See supplementary data 1 (section 1.4.3, Figs. S.1.4, and S.1.5) for mathematical explanation and more details on each of the inputs to the FE models.

More specifically, the only kinematic input to the FE models was the knee flexion angle, since it has been shown that marker-based motion analysis is accurate for measuring the knee flexion angle, but inaccurate for estimating knee secondary kinematics [51]. Nonetheless, the MS model of the study had a moving knee flexion/extension axis of rotation (defined as a function of knee flexion angle) [50], [52], intended to account for knee secondary kinematics due to the interaction of ligaments. This moving axis could potentially affect muscle moment arms, muscle activations, and the estimated knee JCF. However, ligament forces did not explicitly appear in the equations of motions solved by the OpenSim joint reaction tool since ligaments were not physically implemented in the MS model [61]. But in the FE models, ligaments were explicitly implemented, and knee secondary kinematics DoFs were unlocked to be governed by the knee kinetics estimated by the associated MS model, accounting for force-dependent interaction of ligaments with the knee kinematics and kinetics (i.e., forward dynamics solution in the FE model, based on inverse dynamics solutions from the MS model). To conclude, no extra energy or duplicate forces/moments were applied to the FE models due to adding ligaments and unlocking knee secondary kinematics DoFs (for more details, see supplementary data 1, section 1.4.3). Importantly, this approach of driving the FE model with the MS model is previously shown to replicate knee kinetics and secondary kinematics consistent with experiments [21], [28], [36], [37].

In the same vein, we should also mention that the muscle force vectors acting on the knee joint were included within the total JCFs calculated by the OpenSim joint reaction analysis toolbox. Hence, muscle forces should not be, and were not, imported into the FE models separately to avoid duplicating their action. Since the JCFs were applied to the center of the joint in the FE models, they generate no moments around the knee joint. Consequently, we imported the knee external moments and the moments generated by the muscles around the joint center into the FE models, in addition to the JCFs, which, to reiterate, meant there was no duplication of muscle moments.

In all the FE models, the bottom of the tibia was fixed. All the nodes located on the interface between the femoral cartilage and subchondral bone were coupled to the femoral reference point (Fig. 1). Likewise, all the nodes located on the interface of patellar cartilage with the subchondral bone were coupled to the patellar reference point (Fig. 1). The tibiofemoral and patellofemoral reference points represent the joints' center of rotation identical to those of the associated MS models, providing consistent incorporation of the loading and boundary conditions into the FE models. The knee flexion angle, knee joint moments (i.e., abduction/adduction and internal/external moments), and tibiofemoral JCFs were applied to the femoral reference point, and the patellar JCF and the moment generated by the quadriceps muscles (i.e., flexion/extension, abduction/adduction and internal/external moments) were applied to the patellar reference point. The femur had 5 active DoFs, and the patella had 6 active DoFs in the FE models. A more detailed presentation of the loading and boundary conditions is provided in supplementary data 1, and our previous study [36].

D. FE Simulations and Post-Processing of the FE Results

Abaqus soils consolidation solver was used that considers quasistatic equilibrium for translational/rotational DoFs and transient response for fluid flow. Consequently, the force-displacement and moment-rotation equations (at each DoF) were always in quasistatic equilibrium during the analysis. In this study, we investigated tibial cartilage center of pressure (CoP), JCF, and tissue mechanical responses comprising: (i) maximum principal stress, (ii) collagen fiber strains, and (iii) maximum shear strain within knee cartilages and menisci.

The tibial, femoral, and patellar cartilage and the menisci were subdivided into several regions to elaborate regional JCF and tissue mechanical responses during the different activities (supplementary data 1, Fig. S.1.6). The subdivision intended to distinguish how different regions of the joint tissue are loaded during a certain activity and give insights into the subject-specific design of rehabilitation protocols, for instance, by (un)loading a region of interest. The medial and lateral tibial cartilages were both subdivided into anterior, central, and posterior regions (Fig. S.1.6-A). The tibial central region was designated with two parallel lines (along the mediolateral knee axis) that included the whole femur-to-tibia cartilage-to-cartilage contact area, but not the menisci-to-tibia contact area, with the subject standing in an extended knee posture (Fig. S.1.6-A). The femoral cartilage was divided into medial and lateral regions, and each of those into central and posterior sub-regions. The central femoral region was defined with a line parallel to the mediolateral knee axis that includes the whole tibia-to-femur and menisci-to-femur contact area when the subject was in a fully extended standing knee posture (Fig. S.1.6-B). The patellofemoral joint was divided into medial and lateral regions, and the medial meniscus and lateral meniscus were analyzed separately (Fig. S.1.6-B). In addition

to the above-mentioned regions, the tibiofemoral joint was also subdivided into a femoral-to-tibial cartilage contact region, and a meniscus-to-tibial cartilage contact region, for both the medial and lateral tibia (Fig. S.1.6-C). It should be mentioned that the last four contact regions (Fig. S.1.6-C) were detected at each time point of every trial.

The elements within each region that were in contact with any other surface regions were detected separately at each time point, and the tissue mechanical responses were extracted for those selected elements. Next, the average of the tissue mechanical responses (e.g., maximum principal stress) at each time point and for the selected elements were calculated, resulting in curves of the instantaneous average tissue mechanical responses over the contact area. From these, the maximum values and the area under the curves (i.e., the time integral called the impulse) were calculated, and the impulse divided by the total trial time called the mean of that parameter (i.e., the average mechanical responses of the trial).

In addition, forces applied to each region in the FE models were also separately calculated by surface integration of the contact pressure over each contact region (i.e., contact pressure multiplied by the contact area). Similar to the tissue mechanical responses, the maximum, the impulse, and the mean of the regional JCF were calculated and analyzed.

E. Statistical Analyses

The statistical analyses were performed on the maximum, the impulse, and the mean for each region of cartilages and menisci. A two-way repeated-measures analysis of variance (ANOVA) was used to investigate the main and interaction effects across regions and tasks on the estimated JCF and tissue mechanical responses. When a significant interaction effect was observed, a one-way repeated-measures ANOVA followed by a multiple-comparison post-hoc correction test (Bonferonni correction) was performed within tasks and regions. The significance level was $p < 0.05$, with all statistical tests being performed in SPSS (IBM Corporation, US).

The estimated results by the SO-based MS-FE models and the EMG-assisted MS-FE models were compared utilizing statistical parametric mapping (SPM) paired t-tests [80] with the significance level of 0.05 along with the Bonferroni correction. Root mean square error (RMSE) and coefficient of determination (R^2) between experimental and predicted muscle excitations, followed by paired t-test, were calculated for each MS modeling approach (see supplementary data 1 section 2.1). Pearson correlation tests were also performed (within MATLAB) to investigate the association between the maximum and impulse of joint-level mechanical loading and maximum and impulse of either regional JCFs or tissue-level mechanical responses for all the study activities (see supplementary data 1 section 2.2).

III. Results

A. Daily Activities

The CoP at the maximum JCF was mostly located in the central tibial cartilage during the gait and pick up, but located within posterior regions during other daily activities (Fig. 2).

No significant differences were observed in the regional tissue mechanics between the habitual and standard gaits and

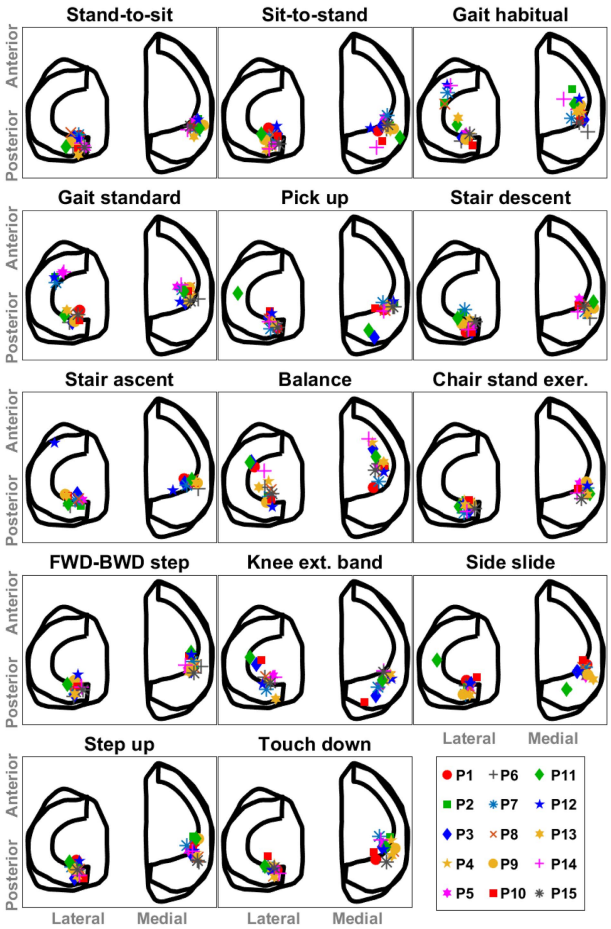

Fig. 2. The tibial cartilage center of pressure (CoP) at the maximum JCF for 15 participants of the study during the daily activities and rehabilitation exercises estimated by the EMG-assisted MS-FE pipeline of the study.

between stand-to-sit and sit-to-stand ($p < 0.02$) (Figs. 3, S.1.7, and S.1.8). The stress, but not the fibril strain and shear strain, during stair ascent was significantly smaller ($p < 0.01$) on the medial central and medial posterior tibial cartilage compared to corresponding values in stair descent (Fig. 3, Figs. S.1.7 and S.1.8). Otherwise, no significant differences were observed in tissue mechanics between stair ascent and descent (Figs. 3, S.1.7, and S.1.8). The maximum principal stress and fibril strain on the central region of the medial tibial cartilage were higher during stair descent ($p < 0.04$) compared to other daily activities, except for stair ascent (Figs. 3 and S.1.7). Tissue mechanics within the central region of the lateral tibial cartilage were smallest during the gait, compared to other daily activities ($p < 0.05$, Figs. 3, S.1.7, and S.1.8).

The maximum principal stress of the central medial femoral condyle cartilage was significantly higher in stair activities compared to other daily activities ($p < 0.01$), but no significant differences were detected in the lateral central region amongst any of the daily activities (Fig. 4). No significant differences were observed for the maximum principal stress of the medial, lateral, or total contact area of the femoral cartilage at the patellofemoral joint in daily activities (Fig. 4). The maximum principal stress of both medial and lateral patella cartilage was significantly ($p < 0.001$) lower during the gait compared to other daily activities (Fig. S.1.9). The greatest tissue mechanical responses ($p < 0.03$) of the menisci were observed in

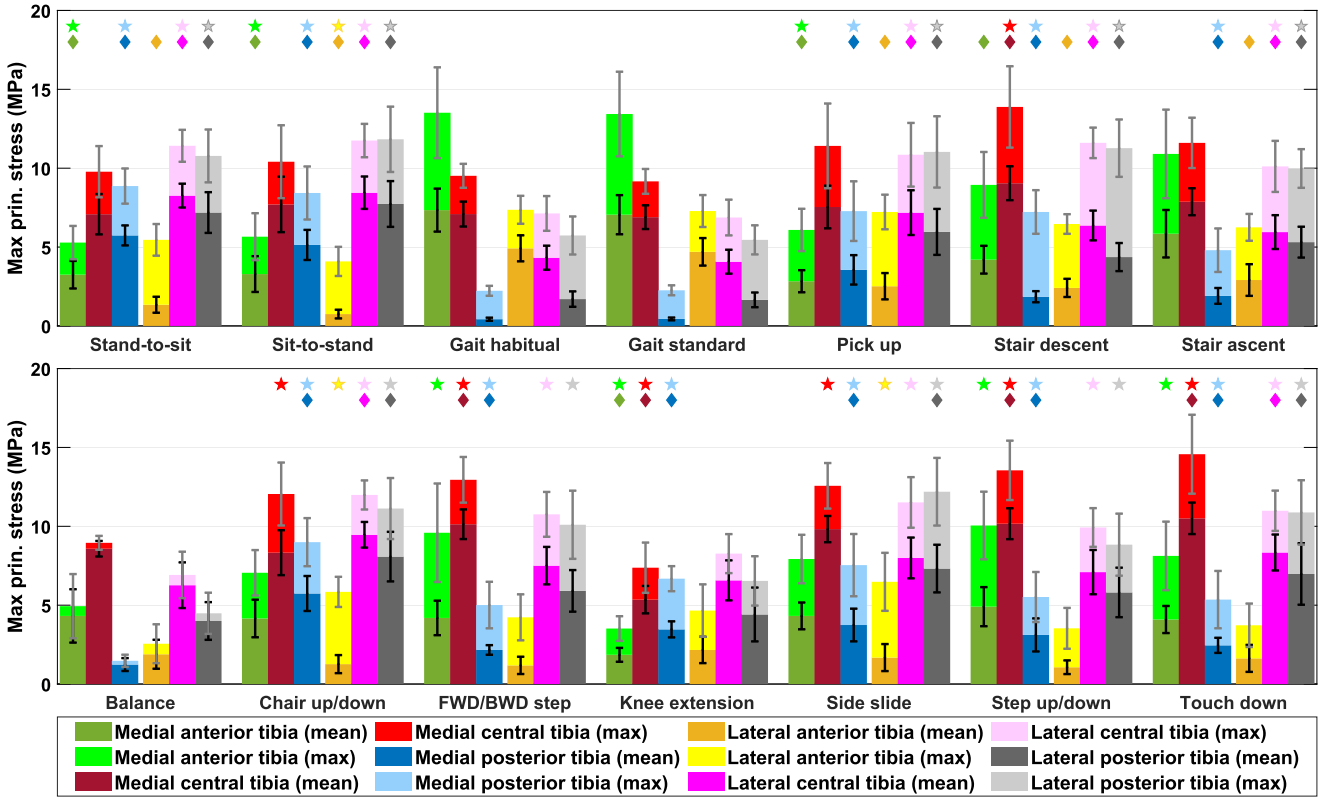

Fig. 3. Max and mean of the maximum principal stress (EMG-assisted MS-FE approach) within the tibial cartilage regions during daily activities (top row) and rehabilitation exercises (bottom row). Stars and diamonds show significant difference ($p < 0.05$) in max and mean of the maximum principal stress compared to those of the gait habitual and balance for daily activities and rehabilitation exercises, correspondingly. Error bars show 95% confidence intervals.

stand-to-sit and sit-to-stand, followed by the pick-up, stair negotiation, and gait (Figs. S.1.10 and S.1.11).

B. Rehabilitation Exercises

Within the lateral tibial cartilage, the CoP at the maximum JCF was mostly at the posterior tibial cartilage across the exercises except for the knee extension (Fig. 2). The CoP at the maximum JCF was mostly within the central medial tibial cartilage in balance, forward/backward step, and touch down, while the CoP at the maximum JCF was more within the posterior medial regions in other exercises (Fig. 2). Compared to other exercises, balance and knee extension exercises evoked equal or significantly smaller tissue mechanical responses in the tibiofemoral and patellofemoral cartilage and menisci (Figs. 3 to 5 and Figs. S.1.7 to S.1.11). Knee extension was the only exercise during which the maximum principal stresses were significantly ($p = 0.016$) greater on the lateral tibial cartilage than on the medial side (Fig. S.1.12).

With the exception of the balance and knee extension exercise, no significant differences between rehabilitation exercises were observed in the maximum of the tissue mechanical responses of the medial central tibial cartilage and also lateral tibial regions (Figs. 3, S.1.7, and S.1.8).

During the balance, forward/backward step, step up/down, and touch down exercises, the maximum of the tissue mechanical responses was significantly ($p < 0.01$) higher on the medial anterior femur than those of the medial posterior femur (Fig. 4). On the lateral femur, the maximum of the tissue mechanical responses was significantly ($p < 0.02$) higher on the posterior femur compared to the anterior femur during all the exercises except for the balance and touch down exercises (Fig. 4). Within the patellar cartilage, the maximum principal stress was the lowest ($p < 0.001$) during balance and knee extension, compared to other exercises (Fig. S.1.9).

C. Comparison of Clinical Evaluations and Joint Mechanics

In ~92% of participants with the diagnosed medial tibiofemoral osteoarthritis (OA), cartilage defect was observed within the femur-to-tibia contact regions of tibial cartilage, instead of meniscus-to-tibial cartilage contact regions (Fig. S.1.2). From simulation results, the JCF impulse and maximum principal stress were significantly ($p < 0.05$) greater on the medial femoral-to-tibial cartilage contact regions, as compared to the medial meniscus-to-tibial cartilage contact regions, during all the daily activities and rehabilitation exercises (Fig. S.1.13 and S.1.14). For the remaining (~8%) of participants with medial tibiofemoral OA, cartilage defects were observed within the femoral cartilage (i.e., the defected area can be located within the femoral-to-tibial or femoral-to-meniscus contact regions). Nonetheless, in these 8% of participants, the maximum of the tissue mechanical responses during different activities was either similar or significantly ($p < 0.005$) higher on the medial femoral cartilage than those of the lateral femoral cartilage (Fig. 4). Likewise, the JCFs and maximum principal stresses on the lateral tibial cartilage were significantly greater on the femoral-to-tibial cartilage contact region compared to the meniscus-to-tibial cartilage contact region (Figs. S.1.13 and S.1.14). However, the difference in the peak magnitudes of the JCFs

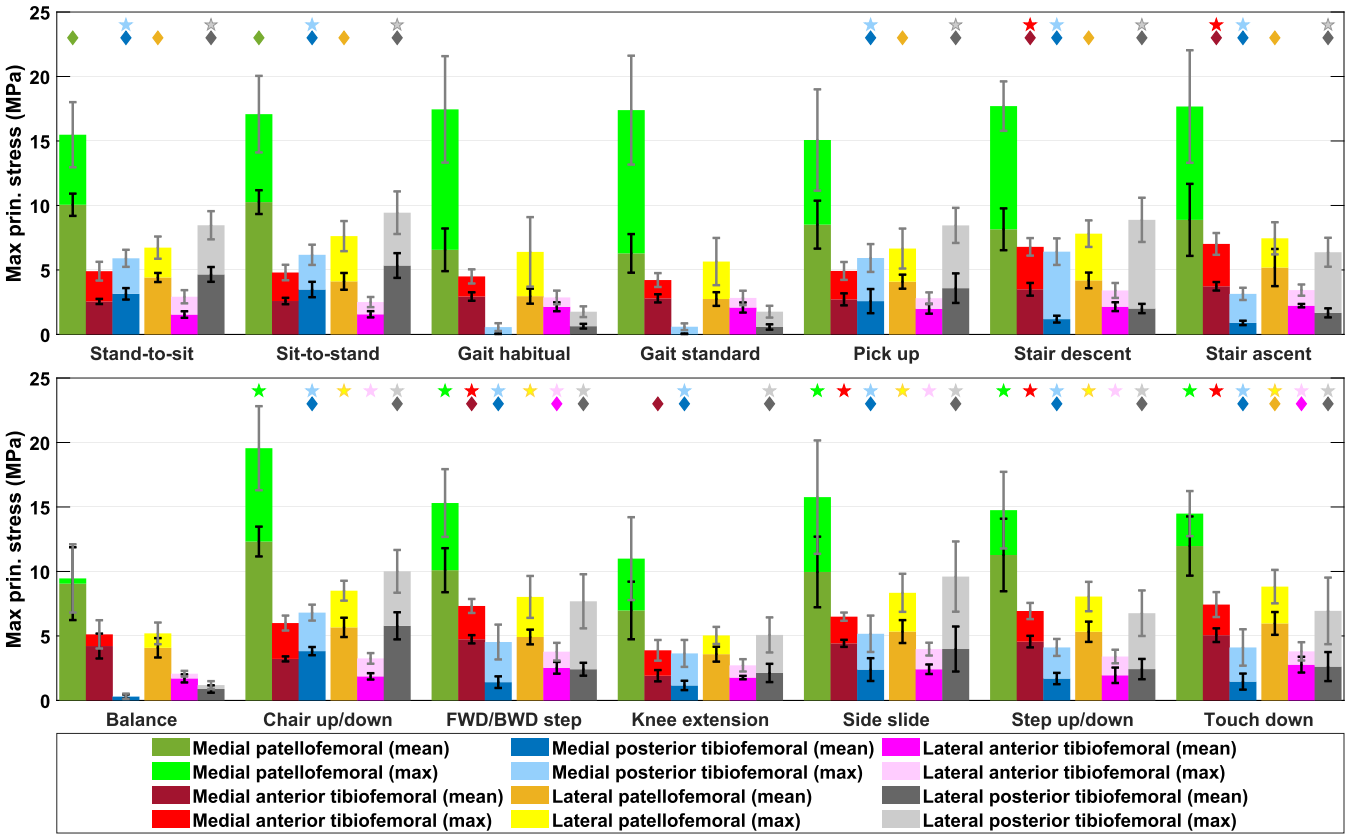

Fig. 4. Max and mean of the maximum principal stress (EMG-assisted MS-FE approach) within the femoral cartilage regions during daily activities (top row) and rehabilitation exercises (bottom row). Stars and diamonds show significant difference ($p < 0.05$) in max and mean of the maximum principal stress compared to those of the gait habitual and balance for daily activities and rehabilitation exercises, correspondingly. Error bars show 95% confidence intervals.

and maximum principal stresses between these two regions on the lateral tibia was much lower compared to that on the medial tibia (Figs. S.1.13 and S.1.14).

Overall, ∼53% of study participants had radiologist diagnosed cartilage defect in the medial tibiofemoral joint, ∼20% in the lateral tibiofemoral joint, and ∼13% in both medial and lateral tibiofemoral joints, while the rest had a combination of tibiofemoral and patellofemoral OA (Fig. S.1.2). Simulation results showed that the JCF impulse was substantially greater on the medial tibial cartilage, compared to the lateral tibial cartilage, during all daily activities and rehabilitation exercises (Fig. S.1.15). Moreover, in all daily activities, except for stand-to-sit, the maximum principal stress was significantly ($p < 0.05$) greater within the medial tibial cartilage compared to the lateral side (Fig. S.1.12).

The radiologist identified an equal incidence of cartilage defects on medial and lateral patellar cartilage across study participants. Our results also showed that the tissue mechanical responses between medial and lateral patellar cartilage were not statistically different ($p > 0.05$) in daily activities and rehabilitation exercises (Fig. S.1.9).

D. Subject-Specific Analysis

In addition to overall differences in joint mechanics across different daily activities and rehabilitation exercises, considerable inter-subject variations were observed. Greater inter-subject variations in EMGs (supplementary data 2), JCFs (supplementary data 3), and tissue mechanical responses were observed in effort-demanding activities (i.e., activities with higher muscle activation levels and JCFs) such as stair negotiation and closed-kinetic-chain exercises, compared to moderate-intensity activities such as stand-to-sit, sit-to-stand, walking, balance, and knee extension (Figs. 3 and 4, and Figs. S.1.7 to S.1.12). On the other hand, the CoP at the maximum JCF showed greater inter-subject variations in moderate-intensity tasks as compared to effort-demanding activities (Fig. 2).

Inter-subject variations were observed in the estimated maximum shear strain and maximum principal stress, which are related to proteoglycan loss and collagen damage (Fig. 5). For example, in participant 3, cartilage defects were observed within the femoral-to-tibial contact region of medial tibial and femoral cartilage surfaces. The forward/backward step showed high shear strain within the medial tibial cartilage compared to other activities (Fig. 5). Also, maximum principal stress distribution showed higher concentrations within the medial tibial cartilage-to-cartilage contact area than those of the lateral tibia during forward/backward step, compared to other selected activities of participant 3 (Fig. 5).

For participant 13, cartilage defects were observed within the cartilage-to-cartilage contact area of the medial tibial cartilage and also on both lateral and medial femoral cartilages (Fig. 5). Our simulations showed higher shear strain within the aforementioned regions (containing cartilage defect) during side slide, compared to other daily activities (Fig. 5). Also, participant 13 had greater stress concentrations within the cartilage-to-cartilage contact area of the medial compartment,

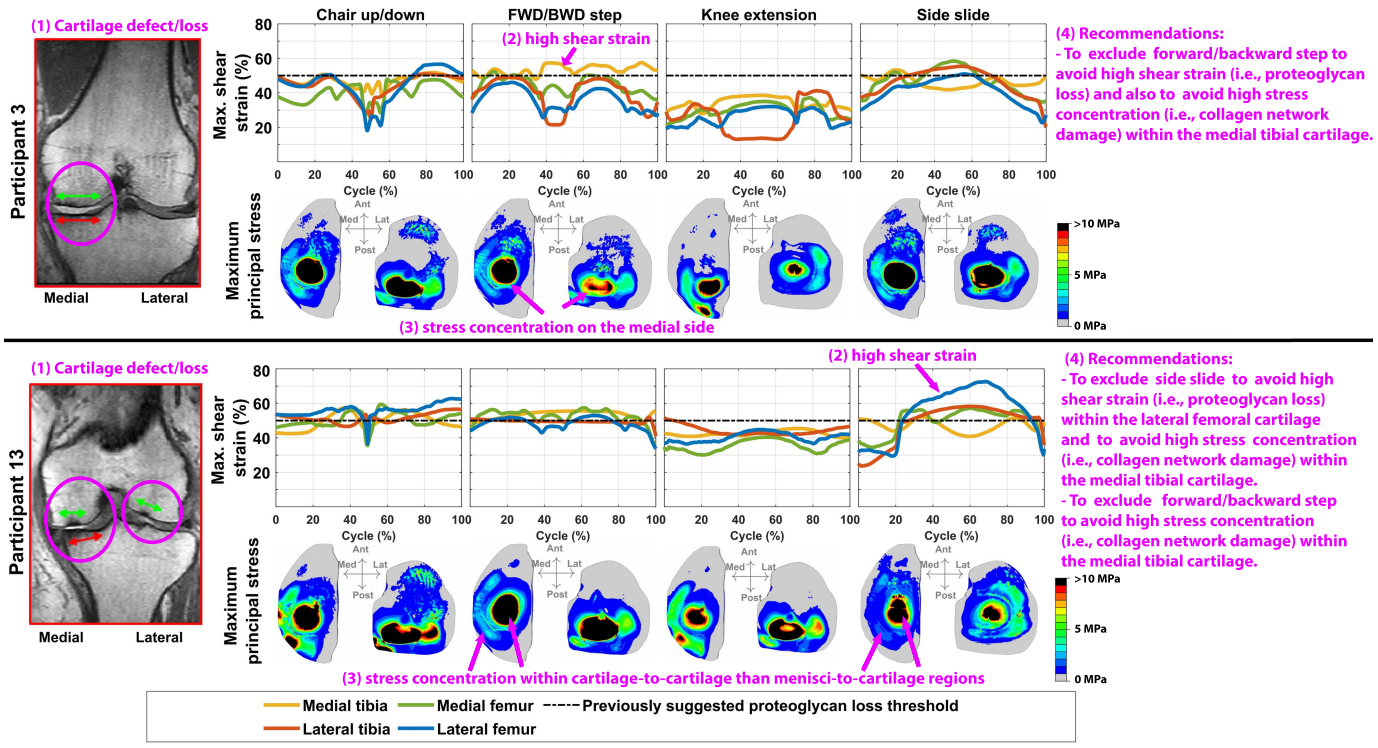

Fig. 5. Cartilage defect/loss regions identified by the radiologist, and the estimated joint mechanics of three randomly-selected participants of the study performing four different rehabilitation exercises. Each sub-figure illustrates 1) on the left: the subjects' cartilage defect/loss regions within the femoral cartilage (in green) and tibial cartilage (in red), 2) on the top row: the peak of the maximum shear strain within the femoral and tibial cartilages during the selected exercises (i.e., indicative of proteoglycan loss), and 3) on the bottom row: the maximum principal (tensile) stress distribution within the tibial cartilage at the time-point of the maximum JCF of the selected activity/subject (i.e., indicative of collagen network damage). The explanations in purple demonstrate examples of subject-specifically tailored rehabilitation protocols to avoid excessive tissue-level loading within the regions of interest.

compared to menisci-to-cartilage contact region, during forward/backward and side slide exercises compared to other exercises (Fig. 5).

IV. Discussion

A. Summary

We utilized a novel semi-automated MS-FE modeling pipeline [36] to investigate detailed knee mechanics during different daily activities and rehabilitation exercises in individuals with KOA. The EMG-assisted MS model accounted for subject-specific muscle activations that are often altered in individuals with MS disorders, e.g., KOA [81]–[85]. In addition, the FE models used a state-of-the-art FRP(V)E soft tissue material model that has been shown to predict mechanically-induced adaptive and degenerative response of fibrillar (collagen) and nonfibrillar (proteoglycans) matrices within the tissue [24], [25].

B. Daily Activities

Cartilage regions that experience excessive tissue mechanical responses may be susceptible to KOA [86]. The greater tissue mechanical responses on medial tibia compared to the lateral tibia during most of daily activities (Fig. S.1.12) may explain the considerably higher prevalence of medial KOA as compared to lateral KOA reported in the literature [87], an outcome also observed in our study's participants (Fig. S.1.2). Moreover, tissue mechanical responses in femur-to-tibia contact regions were significantly greater in magnitude ($p < 0.01$) compared to those in the meniscus-to-tibia contact regions (Fig. S.1.14). This may account for the higher incidence of cartilage defects in femur-to-tibia cartilage contact regions than in meniscus-to-tibial cartilage contact regions that were diagnosed in our study participants (Fig. S.1.2).

Previous studies have shown that excessive magnitude and duration of tissue stress can damage the collagen fibrillar network [40]. Both peak and mean (over loading-duration) of the maximum principal stress within knee cartilages and menisci were similar or lower during walking compared to other daily activities and dynamic weight-bearing rehabilitation exercises (Figs. 3, 4, S.1.9, and S.1.10). Accordingly, walking may be suggested as a moderate-intensity physical activity to reduce rates of chronic diseases [88] with a low risk of collagen network deterioration stemming from the relatively small tissue stress. Nonetheless, with respect to the daily activities, stair negotiation was responsible for the greatest JCFs and tissue mechanical responses (Fig. 3 and S.1.15) within the tibial cartilage. This may account for the reduced functional status and increased subjective pain in the KOA individuals going up or down stairs [89].

C. Rehabilitation Exercises

Quadriceps weakness is a known risk factor for the incidence and progression of KOA, and can significantly influence the success rate of knee surgeries such as total knee replacement [90]. Among the exercises studied, the smallest regional tissue mechanical responses were observed in the

knee extension exercise (Figs. 3 to 5). Hence, the knee extension exercise may be recommended as an effective muscle strengthening protocol [11], [12] for patients suffering from cartilage defect/loss since it minimizes tissue mechanical responses (Figs. 3 to 5). The knee extension exercise was also the only exercise with significantly greater tissue mechanical responses on the lateral tibial cartilage than on the medial tibial cartilage (Fig. S.1.12), compared to closed-kinetic-chain exercises. It may be proposed that open-kinetic-chain exercises confer more freedom of manipulating localized joint loading due to having more control over the external forces/moments applied to the limbs. Nonetheless, more studies on different open-kinetic-chain exercises are required using the presented simulation methods.

The balance exercise has been designed to improve proprioception and subsequent control of knee motion in KOA subjects [91]. When compared to the other rehabilitation exercises, the balance exercise elicited wider inter-subject variations in EMGs (supplementary data 2), JCFs (supplementary data 3), and also in the location of the CoP at the maximum JCF (Fig. 2). These inter-subject variations may be attributed to the different muscle recruitment strategies used to reduce knee pain while maintaining balance. Nonetheless, the tissue mechanical responses during the balance exercises were the smallest of all the closed-kinetic-chain exercises (Fig. 3 and 4). This may indicate balance exercise can improve proprioception, knee neuromuscular control, and the patients' functional capacities [91] while not necessarily evoking excessive tissue mechanical responses that would potentially accelerate the progression of KOA [24], [25], [40].

D. Subject-Specific Design of Rehabilitation Protocols

Knee (un)loading strategies in individuals with KOA may be more associated with their functional status (e.g., limited by muscle strength) rather than symptoms (e.g., pain perception) [89], [92]. In other words, individuals with KOA often have limited capability, due to muscle weakness [90], [93], to alter their muscle recruitment strategy and control joint alignments, for instance, to unload the OA affected regions and reduce pain while performing effort-demanding activities [89], [92]. Supporting this hypothesis, we observed similar loading locations (CoP) across the participants in effort-demanding tasks but more variations in the loading locations in moderate-intensity tasks (Fig. 2). Hence, in effort-demanding tasks (and most probably when muscle weakness and lack of joint control is present), it may be even more important to aim for subject-specifically tailored rehabilitation protocols to avoid excessive loading of OA affected regions and potentially lower the risk for mechanically-induced degradation of the joint's load-bearing tissue. Moreover, as the site of cartilage degeneration, muscle strength and activation, and movement patterns are all unique to the individual, using the simulation approach to personalize rehabilitation is prudent, and we have shown it is feasible.

The clinical utility of the workflow is to provide clinicians with their client's joint mechanics such that they can optimize rehabilitation protocols to avoid excessive tissue mechanics causing soft tissue degradation. We showcased the feasibility of this workflow using the example of peak maximum shear strain within tibial and femoral cartilages (Fig. 5) in four exercises (including open- and closed-kinetic-chain exercises) performed by two randomly selected participants. The maximum shear strain has been previously suggested to indicate cartilage degradation due to cell death and fixed charged density loss of proteoglycans [24], [26]. The maximum principal stress distribution at the time of the maximum JCF (illustrated in Fig. 5) has been shown as an indicator of collagen network damage [40]. In addition, discussions on the capabilities of the devised workflow to incorporate subject's muscle activation patterns within the analyses (e.g., compared to the conventional SO-based neural solution) are provided in section 2 of supplementary data 1.

Participant 3 was diagnosed with medial KOA (Fig. 5). Our simulation results (Fig. 5) suggested this participant should avoid forward/backward step due to high maximum shear strains within the medial compartment due to the potential for cartilage degradation. Likewise, the CoP at the maximum JCF during forward/backward step was located within the region with diagnosed cartilage defect/loss (Figs. 2 and 5), potentially exacerbating these injuries. In contrast, chair up/down, knee extension, and side slide exercises did not impose excessive tissue mechanics on cartilage defect regions for participant 3 (Fig. 5).

Participant 13 was diagnosed with medial tibial and femoral KOA and lateral femoral KOA (Fig. 5). Accordingly, the subject may be recommended to avoid side slide and forward/backward step exercises due to high maximum shear strains (considering the magnitudes and loading time) and higher stress concentration on the femoral-to-tibial cartilage contact regions to potentially slow cartilage degradation (Fig. 5).

E. Limitations

The participants were not grouped clinically, e.g., based on KOA grade. This was because our goal was to investigate the localized joint loading in various activities in patients with KOA regardless of the association between the other factors that may influence, e.g., the EMGs and joint mechanics. Results showed that the devised pipeline has the potential to analyze multi-level joint mechanics of individuals with different levels of KOA due to the inclusion of subject's kinematics, kinetics, and muscle activation patterns. Nonetheless, complimentary evaluations with larger cohorts will be needed to determine if the localized joint loading is specific to different populations.

As a potential limitation, the MS model of the study did not physically include certain elements, such as knee ligaments. Nevertheless, the knee joint had a moving flexion/extension axis to replicate the interaction of ligaments with knee secondary kinematics [52]. Importantly, the MS model has been developed to estimate muscle moment arms and muscle activation levels comparable with experiments [50], [94]. Finally, the explicit interaction of ligaments with knee JCFs was considered in the FE model of the study. In addition, the muscle-tendon parameters of the devised MS models

were not subject-specific. Nevertheless, the calibration within the CEINMS using the subject's EMG envelopes and joint moments has been shown to attenuate the effect of the muscle-tendon uncertainties on the simulation results [95]. Also, material parameters of the knee cartilage and menisci may vary in patients and also at different joint sites that can alter the magnitude of the local tissue mechanical responses [96]. However, no practical methods are available to fully extract the subject's soft tissue mechanical properties, and hence, the material parameters utilized in this study were adopted from the literature. This also enabled us to explore alterations in tissue mechanics due to changes in knee loading and not due to altered regional material parameters. Subject- and site-specific structural properties of cartilage have been earlier implemented in the FE model from MRI, although that workflow is highly time-consuming [96].

The atlas-based FE modeling approach has been favorably evaluated and validated against the follow-up data (i.e., KOA progression) [67]. Here this approach was updated to include also patella. Only one template, instead of several, was used since it was shown earlier to work well [67]. Nonetheless, estimation of local tissue mechanical responses around cartilage lesions, in general, is a noted limitation of the atlas-based modeling approach [97]. Importantly, our musculoskeletal radiologist observed no knee cartilage lesions in our study participants. Currently, the inclusion of subject-specific cartilage lesions requires lengthy manual mesh editing. Our future studies aim to enhance the atlas-based FE modeling method and include subject's tissue lesions employing multi-template approaches and nonlinear scaling methods such as statistical shape modeling [98].

F. Clinical Utility and Future Developments

Scaling the MS models (using OpenSim scaling toolbox taking, on average, up to 30 minutes) and measuring the subject's anatomical dimensions (taking, on average, up to 10 minutes) were performed manually. For this reason, the pipeline was named semi-automated. Importantly, creating the FE models for each study participant took only several minutes, with minimum user effort and input, compared to traditional manual modeling, which takes several weeks of an expert user with a high level of unique skills [28], [36]. Multi-DoFs calibration of the MS model took ∼4 hours per subject (including all 14 tasks within the calibration). Then the automated MS-FE analysis and delivering the results took, on average, ∼20 hours for each activity analyzed (using a typical computer and single-thread analysis), which seems a reasonable amount of time for clinical use compared to regular tests such as complete blood count that can take up to several days to deliver the results. Nonetheless, multi-core analyses and cloud computing may provide analysis of several trials in less than a day.

Though, several burdens on practical use of the employed workflow, such as the need for 3D motion capture, subject's MRIs, and solving convergence issues of the models should be solved, for which we have extensively planned our future studies using surrogate modeling and machine learning algorithms [98], [99]. Importantly, we plan to reduce the simulation time towards real-time MS-FE analysis, make the whole pipeline fully-automatic, incorporate subject's lesions with the FE model geometries, and finally, release the toolbox for clinical use. Also, we aim to incorporate our developed and validated cartilage degradation algorithms [24], [100] within the pipeline to provide predictive evaluations.

V. Conclusion

Herein we demonstrated the utilization of a semi-automated modeling and simulation pipeline of the knee and characterized joint mechanics in different activities and rehabilitation exercises of individuals with KOA. We provided compelling evidence showcasing the usability of the developed pipeline for various tasks and patients in different levels of KOA, as well as the potential for implementing the pipeline as a feasible and rapid MS-FE analysis toolbox for subject-specific design of functional activities, considering tissue remodeling and degeneration responses. From the tissue remodeling perspective, clinicians and therapists can consider the tissue mechanics within different regions of the joint and fibrillar or nonfibrillar matrices of the tissue to optimally load the joint when designing the subject's rehabilitation protocol or modifications in different activities.

Appendix

More information on the method and results are presented in supplementary data 1 to 4.

References

[1] E. Losina *et al.*, "Lifetime risk and age at diagnosis of symptomatic knee osteoarthritis in the U.S.," *Arthritis Care Res.*, vol. 65, no. 5, pp. 703–711, May 2013, doi: 10.1002/acr.21898.

[2] T. Miyazaki, M. Wada, H. Kawahara, M. Sato, H. Baba, and S. Shimada, "Dynamic load at baseline can predict radiographic disease progression in medial compartment knee osteoarthritis," *Ann. Rheum. Dis.*, vol. 61, no. 7, pp. 22–617, Jul. 2002, doi: 10.1136/ard.61.7.617.

[3] W. Wilson, C. van Burken, C. C. van Donkelaar, P. Buma, B. van Rietbergen, and R. Huiskes, "Causes of mechanically induced collagen damage in articular cartilage," *J. Orthopaedic Res.*, vol. 24, no. 2, pp. 220–228, Dec. 2006, doi: 10.1002/jor.20027.

[4] E. Alentorn-Geli *et al.*, "Prevention of non-contact anterior cruciate ligament injuries in soccer players. Part 1: Mechanisms of injury and underlying risk factors," *Knee Surgery, Sports Traumatol., Arthroscopy*, vol. 17, no. 7, pp. 705–729, Jul. 2009, doi: 10.1007/s00167-009-0813-1.

[5] D. T. Felson, "Osteoarthritis as a disease of mechanics," *Osteoarthritis Cartilage*, vol. 21, no. 1, pp. 10–15, Jan. 2013, doi: 10.1016/j.joca.2012.09.012.

[6] P. K. Edwards, T. Ackland, and J. R. Ebert, "Clinical rehabilitation guidelines for matrix-induced autologous chondrocyte implantation on the tibiofemoral joint," *J. Orthopaedic Sports Phys. Therapy*, vol. 44, no. 2, pp. 102–119, Feb. 2014, doi: 10.2519/jospt.2014.5055.

[7] S. van Grinsven, R. E. H. van Cingel, C. J. M. Holla, and C. J. M. van Loon, "Evidence-based rehabilitation following anterior cruciate ligament reconstruction," *Knee Surgery, Sports Traumatol., Arthroscopy*, vol. 18, no. 8, pp. 1128–1144, Jan. 2010, doi: 10.1007/s00167-009-1027-2.

[8] M. A. Yabroudi and J. J. Irrgang, "Rehabilitation and return to play after anatomic anterior cruciate ligament reconstruction," *Clinics Sports Med.*, vol. 32, no. 1, pp. 165–175, Jan. 2013, doi: 10.1016/j.csm.2012.08.016.

[9] C. M. Dzialo, M. Mannisi, K. S. Halonen, M. de Zee, J. Woodburn, and M. S. Andersen, "Gait alteration strategies for knee osteoarthritis: A comparison of joint loading via generic and patient-specific musculoskeletal model scaling techniques," *Int. Biomechanics*, vol. 6, no. 1, pp. 54–65, Jan. 2019, doi: 10.1080/23335432.2019.1629839.

[10] G. D. Deyle *et al.*, "Physical therapy versus glucocorticoid injection for osteoarthritis of the knee," *New England J. Med.*, vol. 382, no. 15, pp. 1420–1429, Apr. 2020, doi: 10.1056/NEJMoa1905877.

[11] G. McGinty, J. J. Irrgang, and D. Pezzullo, "Biomechanical considerations for rehabilitation of the knee," *Clin. Biomech.*, vol. 15, no. 3, pp. 160–166, Mar. 2000, doi: 10.1016/S0268-0033(99)00061-3.

[12] E. S. Grood, W. J. Suntay, F. R. Noyes, and D. L. Butler, "Biomechanics of the knee-extension exercise. Effect of cutting the anterior cruciate ligament," *J. Bone Joint Surg.*, vol. 66, no. 5, pp. 725–734, Jun. 1984, doi: 10.2106/00004623-198466050-00011.

[13] J. R. Ebert, D. G. Lloyd, D. J. Wood, and T. R. Ackland, "Isokinetic knee extensor strength deficit following matrix-induced autologous chondrocyte implantation," *Clin. Biomech.*, vol. 27, no. 6, pp. 588–594, Jul. 2012, doi: 10.1016/j.clinbiomech.2012.01.006.

[14] I. Eitzen, H. Grindem, A. Nilstad, H. Moksnes, and M. A. Risberg, "Quantifying quadriceps muscle strength in patients with ACL injury, focal cartilage lesions, and degenerative meniscus tears: Differences and clinical implications," *Orthop. J. Sport. Med.*, vol. 4, no. 10, Oct. 2016, Art. no. 2325967116667717, doi: 10.1177/2325967116667717.

[15] S. Løken, T. C. Ludvigsen, T. Høysveen, I. Holm, L. Engebretsen, and F. P. Reinholt, "Autologous chondrocyte implantation to repair knee cartilage injury: Ultrastructural evaluation at 2 years and long-term follow-up including muscle strength measurements," *Knee Surgery, Sports Traumatol., Arthroscopy*, vol. 17, no. 11, pp. 1278–1288, Jul. 2009, doi: 10.1007/s00167-009-0854-5.

[16] R. Tanaka, T. Hayashizaki, R. Taniguchi, J. Kobayashi, and T. Umehara, "Effect of an intensive functional rehabilitation program on the recovery of activities of daily living after total knee arthroplasty: A multicenter, randomized, controlled trial," *J. Orthopaedic Sci.*, vol. 25, no. 2, pp. 285–290, Mar. 2020, doi: 10.1016/j.jos.2019.04.009.

[17] K. L. L. Bennell, M. Hall, and R. S. S. Hinman, "Osteoarthritis year in review 2015: Rehabilitation and outcomes," *Osteoarthritis Cartilage*, vol. 24, no. 1, pp. 58–70, 2016.

[18] B. J. Fregly *et al.*, "Grand challenge competition to predict *in vivo* knee loads," *J. Orthopaedic Res.*, vol. 30, no. 4, pp. 503–513, Apr. 2012, doi: 10.1002/jor.22023.

[19] I. Kutzner *et al.*, "Loading of the knee joint during activities of daily living measured *in vivo* in five subjects," *J. Biomech.*, vol. 43, no. 11, pp. 2164–2173, Aug. 2010, doi: 10.1016/j.jbiomech.2010.03.046.

[20] S. Gilbert, T. Chen, I. D. Hutchinson, D. Choi, C. Voigt, R. F. Warren, and S. A. Maher, "Dynamic contact mechanics on the tibial plateau of the human knee during activities of daily living," *J. Biomech.*, vol. 47, no. 9, pp. 2006–2012, Jun. 2014, doi: 10.1016/j.jbiomech.2013.11.003.

[21] A. Esrafilian *et al.*, "12 degrees of freedom muscle force driven fibril-reinforced poroviscoelastic finite element model of the knee joint," *IEEE Trans. Neural Syst. Rehabil. Eng.*, vol. 29, pp. 123–133, 2021, doi: 10.1109/TNSRE.2020.3037411.

[22] H. Marouane, A. Shirazi-Adl, and M. Adouni, "3D active-passive response of human knee joint in gait is markedly altered when simulated as a planar 2D joint," *Biomech. Model. Mechanobiol.*, vol. 16, no. 2, pp. 693–703, 2017, doi: 10.1007/s10237-016-0846-6.

[23] R. L. Lenhart, J. Kaiser, C. R. Smith, and D. G. Thelen, "Prediction and validation of load-dependent behavior of the tibiofemoral and patellofemoral joints during movement," *Ann. Biomed. Eng.*, vol. 43, no. 11, pp. 2675–2685, Nov. 2015, doi: 10.1007/s10439-015-1326-3.

[24] A. S. A. Eskelinen *et al.*, "Mechanobiological model for simulation of injured cartilage degradation via pro-inflammatory cytokines and mechanical stimulus," *PLOS Comput. Biol.*, vol. 16, no. 6, Jun. 2020, Art. no. e1007998, doi: 10.1371/journal.pcbi.1007998.

[25] S. M. Hosseini, W. Wilson, K. Ito, and C. C. van Donkelaar, "A numerical model to study mechanically induced initiation and progression of damage in articular cartilage," *Osteoarthritis Cartilage*, vol. 22, no. 1, pp. 95–103, Jan. 2014, doi: 10.1016/J.JOCA.2013.10.010.

[26] G. A. Orozco *et al.*, "Prediction of local fixed charge density loss in cartilage following ACL injury and reconstruction: A computational proof-of-concept study with MRI follow-up," *J. Orthopaedic Res.*, vol. 39, no. 5, pp. 1064–1081, May 2021, doi: 10.1002/jor.24797.

[27] O. Klets, M. E. Mononen, P. Tanska, M. T. Nieminen, R. K. Korhonen, and S. Saarakkala, "Comparison of different material models of articular cartilage in 3D computational modeling of the knee: Data from the Osteoarthritis Initiative (OAI)," *J. Biomech.*, vol. 49, no. 16, pp. 3891–3900, Dec. 2016, doi: 10.1016/J.JBIOMECH.2016.10.025.

[28] P. O. Bolcos *et al.*, "Comparison between kinetic and kinetic-kinematic driven knee joint finite element models," *Sci. Rep.*, vol. 8, no. 1, pp. 1–11, Dec. 2018, doi: 10.1038/s41598-018-35628-5.

[29] W. Mesfar and A. Shirazi-Adl, "Biomechanics of the knee joint in flexion under various quadriceps forces," *Knee*, vol. 12, no. 6, pp. 424–434, Dec. 2005, doi: 10.1016/J.KNEE.2005.03.004.

[30] A. Shirazi-Adl and W. Mesfar, "Effect of tibial tubercle elevation on biomechanics of the entire knee joint under muscle loads," *Clin. Biomech.*, vol. 22, no. 3, pp. 344–351, Mar. 2007, doi: 10.1016/J.CLINBIOMECH.2006.11.003.

[31] W. Mesfar and A. Shirazi-Adl, "Knee joint biomechanics in open-kinetic-chain flexion exercises," *Clin. Biomech.*, vol. 23, no. 4, pp. 477–482, May 2008, doi: 10.1016/J.CLINBIOMECH.2007.11.016.

[32] A. Navacchia, D. R. Hume, P. J. Rullkoetter, and K. B. Shelburne, "A computationally efficient strategy to estimate muscle forces in a finite element musculoskeletal model of the lower limb," *J. Biomech.*, vol. 84, pp. 94–102, Feb. 2019, doi: 10.1016/j.jbiomech.2018.12.020.

[33] I. Eskinazi and B. J. Fregly, "A computational framework for simultaneous estimation of muscle and joint contact forces and body motion using optimization and surrogate modeling," *Med. Eng. Phys.*, vol. 54, pp. 56–64, Apr. 2018, doi: 10.1016/j.medengphy.2018.02.002.

[34] K. S. Halonen, C. M. Dzialo, M. Mannisi, M. S. Venäläinen, M. de Zee, and M. S. Andersen, "Workflow assessing the effect of gait alterations on stresses in the medial tibial cartilage–combined musculoskeletal modelling and finite element analysis," *Sci. Rep.*, vol. 7, no. 1, pp. 1–14, Dec. 2017, doi: 10.1038/s41598-017-17228-x.

[35] H. Marouane, A. Shirazi-Adl, and M. Adouni, "Alterations in knee contact forces and centers in stance phase of gait: A detailed lower extremity musculoskeletal model," *J. Biomech.*, vol. 49, no. 2, pp. 185–192, Jan. 2016, doi: 10.1016/j.jbiomech.2015.12.016.

[36] A. Esrafilian *et al.*, "An EMG-assisted muscle-force driven finite element analysis pipeline to investigate joint- and tissue-level mechanical responses in functional activities: Towards a rapid assessment toolbox," *IEEE Trans. Biomed. Eng.*, early access, p. 1, 2022, doi: 10.1109/TBME.2022.3156018.

[37] A. Esrafilian, L. Stenroth, M. E. Mononen, P. Tanska, J. Avela, and R. K. Korhonen, "EMG-assisted muscle force driven finite element model of the knee joint with fibril-reinforced poroelastic cartilages and menisci," *Sci. Rep.*, vol. 10, no. 1, p. 3026, Dec. 2020, doi: 10.1038/s41598-020-59602-2.

[38] S. van Rossom, C. R. Smith, D. G. Thelen, B. Vanwanseele, D. Van Assche, and I. Jonkers, "Knee joint loading in healthy adults during functional exercises: Implications for rehabilitation guidelines," *J. Orthopaedic Sports Phys. Therapy*, vol. 48, no. 3, pp. 162–173, Mar. 2018, doi: 10.2519/jospt.2018.7459.

[39] S. C. Starkey *et al.*, "Effect of exercise on knee joint contact forces in people following medial partial meniscectomy: A secondary analysis of a randomised controlled trial," *Gait Posture*, vol. 79, pp. 203–209, Jun. 2020, doi: 10.1016/j.gaitpost.2020.04.025.

[40] M. K. Liukkonen *et al.*, "Evaluation of the effect of bariatric surgery-induced weight loss on knee gait and cartilage degeneration," *J. Biomech. Eng.*, vol. 140, no. 4, pp. 041008-1–041008-11, Apr. 2018, doi: 10.1115/1.4038330.

[41] P. Gerus *et al.*, "Subject-specific knee joint geometry improves predictions of medial tibiofemoral contact forces," *J. Biomech.*, vol. 46, no. 16, pp. 2778–2786, Nov. 2013, doi: 10.1016/j.jbiomech.2013.09.005.

[42] J. C. Ihn, S. J. Kim, and I. H. Park, "*In vitro* study of contact area and pressure distribution in the human knee after partial and total meniscectomy," *Int. Orthopaedics*, vol. 17, no. 4, pp. 214–218, Aug. 1993, doi: 10.1007/BF00194181.

[43] J. T. Mäkelä, S.-K. Han, W. Herzog, and R. Korhonen, "Very early osteoarthritis changes sensitively fluid flow properties of articular cartilage," *J. Biomech.*, vol. 48, no. 12, pp. 3369–3376, Sep. 2015, doi: 10.1016/J.JBIOMECH.2015.06.010.

[44] L. P. Li and K. B. Gu, "Reconsideration on the use of elastic models to predict the instantaneous load response of the knee joint," *Proc. Inst. Mech. Eng. H, J. Eng. Med.*, vol. 225, no. 9, pp. 888–896, Sep. 2011, doi: 10.1177/0954411911412464.

[45] A. Shirazi-Adl, "On the fibre composite material models of disc annulus-comparison of predicted stresses," *J. Biomech.*, vol. 22, no. 4, pp. 357–365, Jan. 1989, doi: 10.1016/0021-9290(89)90050-X.

[46] R. Altman *et al.*, "Development of criteria for the classification and reporting of osteoarthritis: Classification of osteoarthritis of the knee," *Arthritis Rheumatism*, vol. 29, no. 8, pp. 1039–1049, Aug. 1986, doi: 10.1002/art.1780290816.

[47] K. L. Bennell *et al.*, "Neuromuscular versus quadriceps strengthening exercise in patients with medial knee osteoarthritis and varus malalignment: A randomized controlled trial," *Arthritis Rheumatol.*, vol. 66, no. 4, pp. 9–950, Apr. 2014, doi: 10.1002/art.38317.

[48] H. J. Hermens *et al.*, "European recommendations for surface electromyography," *Roessingh Res. Dev.*, vol. 8, no. 2, pp. 8–11, 1999, doi: 10.1016/S1050-6411(00)00027-4.

[49] H. X. Hoang, L. E. Diamond, D. G. Lloyd, and C. Pizzolato, "A calibrated EMG-informed neuromusculoskeletal model can appropriately account for muscle co-contraction in the estimation of hip joint contact forces in people with hip osteoarthritis," *J. Biomech.*, vol. 83, pp. 134–142, Jan. 2019, doi: 10.1016/j.jbiomech.2018.11.042.

[50] D. S. Catelli, M. Wesseling, I. Jonkers, and M. Lamontagne, "A musculoskeletal model customized for squatting task," *Comput. Methods Biomech. Biomed. Eng.*, vol. 22, no. 1, pp. 21–24, Jan. 2019, doi: 10.1080/10255842.2018.1523396.

[51] D. L. Benoit, D. K. Ramsey, M. Lamontagne, L. Xu, P. Wretenberg, and P. Renström, "Effect of skin movement artifact on knee kinematics during gait and cutting motions measured *in vivo*," *Gait Posture*, vol. 24, no. 2, pp. 64–152, Oct. 2006, doi: 10.1016/j.gaitpost.2005.04.012.

[52] P. S. Walker, J. S. Rovick, and D. D. Robertson, "The effects of knee brace Hinge design and placement on joint mechanics," *J. Biomech.*, vol. 21, no. 11, pp. 965–974, Jan. 1988, doi: 10.1016/0021-9290(88)90135-2.

[53] M. A. Marra *et al.*, "A subject-specific musculoskeletal modeling framework to predict *in vivo* mechanics of total knee arthroplasty," *J. Biomech. Eng.*, vol. 137, no. 2, Feb. 2015, Art. no. 020904, doi: 10.1115/1.4029258.

[54] D. G. Lloyd and T. S. Buchanan, "Strategies of muscular support of varus and valgus isometric loads at the human knee," *J. Biomech.*, vol. 34, no. 10, pp. 1257–1267, Oct. 2001, doi: 10.1016/S0021-9290(01)00095-1.

[55] S. L. Delp, "OpenSim: Open-source software to create and analyze dynamic simulations of movement," in *Proc. IEEE Trans. Biomed. Eng.* vol. 54, no. 11, pp. 1940–1950, Oct. 2007.

[56] M. Yamagata, M. Taniguchi, H. Tateuchi, M. Kobayashi, and N. Ichihashi, "The effects of knee pain on knee contact force and external knee adduction moment in patients with knee osteoarthritis," *J. Biomech.*, vol. 123, Jun. 2021, Art. no. 110538, doi: 10.1016/j.jbiomech.2021.110538.

[57] A. Mündermann, C. O. Dyrby, and T. P. Andriacchi, "A comparison of measuring mechanical axis alignment using three-dimensional position capture with skin markers and radiographic measurements in patients with bilateral medial compartment knee osteoarthritis," *Knee*, vol. 15, no. 6, pp. 480–485, Dec. 2008.

[58] T. Matsumoto *et al.*, "A radiographic analysis of alignment of the lower extremities–initiation and progression of varus-type knee osteoarthritis," *Osteoarthritis Cartilage*, vol. 23, no. 2, pp. 217–223, Feb. 2015, doi: 10.1016/j.joca.2014.11.015.

[59] M. Adouni and A. Shirazi-Adl, "Partitioning of knee joint internal forces in gait is dictated by the knee adduction angle and not by the knee adduction moment," *J. Biomech.*, vol. 47, no. 7, pp. 1696–1703, May 2014, doi: 10.1016/j.jbiomech.2014.02.028.

[60] Z. F. Lerner, M. S. DeMers, S. L. Delp, and R. C. Browning, "How tibiofemoral alignment and contact locations affect predictions of medial and lateral tibiofemoral contact forces," *J. Biomech.*, vol. 48, no. 4, pp. 644–650, Feb. 2015, doi: 10.1016/j.jbiomech.2014.12.049.

[61] K. M. Steele, M. S. DeMers, M. H. Schwartz, and S. L. Delp, "Compressive tibiofemoral force during crouch gait," *Gait Posture*, vol. 35, no. 4, pp. 556–560, Apr. 2012, doi: 10.1016/j.gaitpost.2011.11.023.

[62] C. Pizzolato *et al.*, "CEINMS: A toolbox to investigate the influence of different neural control solutions on the prediction of muscle excitation and joint moments during dynamic motor tasks," *J. Biomech.*, vol. 48, no. 14, pp. 3929–3936, Nov. 2015, doi: 10.1016/J.JBIOMECH.2015.09.021.

[63] M. Sartori, M. Reggiani, D. Farina, and D. G. Lloyd, "EMG-driven forward-dynamic estimation of muscle force and joint moment about multiple degrees of freedom in the human lower extremity," *PLoS ONE*, vol. 7, no. 12, Dec. 2012, Art. no. e52618, doi: 10.1371/journal.pone.0052618.

[64] T. S. Buchanan, D. G. Lloyd, K. Manal, and T. F. Besier, "Neuromusculoskeletal modeling: Estimation of muscle forces and joint moments and movements from measurements of neural command," *J. Appl. Biomech.*, vol. 20, no. 4, pp. 95–367, Nov. 2004. Accessed: Jul. 22, 2019. [Online]. Available: http://www.ncbi.nlm.nih.gov/pubmed/16467928

[65] D. G. Lloyd and T. F. Besier, "An EMG-driven musculoskeletal model to estimate muscle forces and knee joint moments *in vivo*," *J. Biomech.*, vol. 36, no. 6, pp. 765–776, Jun. 2003, doi: 10.1016/S0021-9290(03)00010-1.

[66] M. Millard, T. Uchida, A. Seth, and S. L. Delp, "Flexing computational muscle: Modeling and simulation of musculotendon dynamics," *J. Biomech. Eng.*, vol. 135, no. 2, pp. 021005-1–021005-11, Feb. 2013, doi: 10.1115/1.4023390.

[67] M. E. Mononen, M. K. Liukkonen, and R. K. Korhonen, "Utilizing atlas-based modeling to predict knee joint cartilage degeneration: Data from the osteoarthritis initiative," *Ann. Biomed. Eng.*, vol. 47, no. 3, pp. 1–13, Dec. 2019, doi: 10.1007/s10439-018-02184-y.

[68] P. Julkunen, P. Kiviranta, W. Wilson, J. S. Jurvelin, and R. K. Korhonen, "Characterization of articular cartilage by combining microscopic analysis with a fibril-reinforced finite-element model," *J. Biomech.*, vol. 40, no. 8, pp. 70–1862, Jan. 2007, doi: 10.1016/j.jbiomech.2006.07.026.

[69] W. Wilson, "A comparison between mechano-electrochemical and biphasic swelling theories for soft hydrated tissues," *J. Biomech. Eng.*, vol. 127, no. 1, p. 158, Mar. 2005, doi: 10.1115/1.1835361.

[70] W. Wilson, C. C. van Donkelaar, B. van Rietbergen, K. Ito, and R. Huiskes, "Erratum to 'Stresses in the local collagen network of articular cartilage: A poroviscoelastic fibril-reinforced finite element study," *J. Biomech.*, vol. 37, no. 3, pp. 357–366, 2004, doi: 10.1016/J.JBIOMECH.2005.04.024.

[71] P. Böttcher, M. Zeissler, J. Maierl, V. Grevel, and G. Oechtering, "Mapping of split-line pattern and cartilage thickness of selected donor and recipient sites for autologous osteochondral transplantation in the canine stifle joint," *Vet. Surg.*, vol. 38, no. 6, pp. 696–704, Aug. 2009, doi: 10.1111/j.1532-950X.2009.00527.x.

[72] D. W. Goodwin, Y. Z. Wadghiri, H. Zhu, C. J. Vinton, E. D. Smith, and J. F. Dunn, "Macroscopic structure of articular cartilage of the tibial plateau: Influence of a characteristic matrix architecture on MRI appearance," *Amer. J. Roentgenol.*, vol. 182, no. 2, pp. 311–318, Feb. 2004, doi: 10.2214/ajr.182.2.1820311.

[73] S. Below, S. P. Arnoczky, J. Dodds, C. Kooima, and N. Walter, "The split-line pattern of the distal femur: A consideration in the orientation of autologous cartilage grafts," *Arthroscopy J. Arthroscopic Related Surg.*, vol. 18, no. 6, pp. 613–617, Jul. 2002, doi: 10.1053/JARS.2002.29877.

[74] A. Benninghoff, "Form und bau der gelenkknorpel in ihren beziehungen zur funktion," *Zeitschrift für Zellforsch*, vol. 2, no. 5, pp. 783–862, 1925, doi: 10.1007/BF00583443.

[75] E. A. Makris, P. Hadidi, and K. A. Athanasiou, "The knee meniscus: Structure-function, pathophysiology, current repair techniques, and prospects for regeneration," *Biomaterials*, vol. 32, no. 30, pp. 7411–7431, Oct. 2011, doi: 10.1016/J.BIOMATERIALS.2011.06.037.

[76] D. F. Villegas, J. A. Maes, S. D. Magee, and T. L. H. Donahue, "Failure properties and strain distribution analysis of meniscal attachments," *J. Biomech.*, vol. 40, no. 12, pp. 2655–2662, Jan. 2007, doi: 10.1016/J.JBIOMECH.2007.01.015.

[77] L. Blankevoort and R. Huiskes, "Ligament-bone interaction in a three-dimensional model of the knee," *J. Biomech. Eng.*, vol. 113, no. 3, pp. 9–263, Aug. 1991, doi: 10.1115/1.2894883.

[78] P. Atkinson, T. Atkinson, C. Huang, and R. Doane, "A comparison of the mechanical and dimensional properties of the human medial and lateral patellofemoral ligaments," in *Proc. 46th Annu. Meeting Orthopaedic Res. Soc.*, 2000, p. 776, Accessed: Aug. 9, 2020. [Online]. Available: https://works.bepress.com/theresa-atkinson/63/

[79] L. Schatzmann, "Effect of cyclic preconditioning on the tensile properties of human quadriceps tendons and patellar ligaments," *Knee Surg., Sports Traumatol,., Arthroscopy*, vol. 6, pp. S56–S61, Apr. 1998, doi: 10.1007/s001670050224.

[80] T. C. Pataky, "Generalized n-dimensional biomechanical field analysis using statistical parametric mapping," *J. Biomech.*, vol. 43, no. 10, pp. 1976–1982, Jul. 2010, doi: 10.1016/j.jbiomech.2010.03.008.

[81] C. L. Hubley-Kozey, N. A. Hill, D. J. Rutherford, M. J. Dunbar, and W. D. Stanish, "Co-activation differences in lower limb muscles between asymptomatic controls and those with varying degrees of knee osteoarthritis during walking," *Clin. Biomech.*, vol. 24, no. 5, pp. 407–414, Jun. 2009, doi: 10.1016/J.CLINBIOMECH.2009.02.005.

[82] L. C. Schmitt and K. S. Rudolph, "Muscle stabilization strategies in people with medial knee osteoarthritis: The effect of instability," *J. Orthopaedic Res.*, vol. 26, no. 9, pp. 1180–1185, Sep. 2008, doi: 10.1002/jor.20619.

[83] S. C. O'Reilly, A. Jones, K. R. Muir, and M. Doherty, "Quadriceps weakness in knee osteoarthritis: The effect on pain and disability," *Ann. Rheumatic Diseases*, vol. 57, no. 10, pp. 588–594, Oct. 1998, doi: 10.1136/ard.57.10.588.

[84] D. Kumar, K. T. Manal, and K. S. Rudolph, "Knee joint loading during gait in healthy controls and individuals with knee osteoarthritis," *Osteoarthritis Cartilage*, vol. 21, no. 2, pp. 298–305, Feb. 2013, doi: 10.1016/J.JOCA.2012.11.008.

[85] B. A. Killen *et al.*, "Individual muscle contributions to tibiofemoral compressive articular loading during walking, running and side-stepping," *J. Biomech.*, vol. 80, pp. 23–31, Oct. 2018, doi: 10.1016/J.JBIOMECH.2018.08.022.

[86] P. O. Bolcos *et al.*, "Identification of locations susceptible to osteoarthritis in patients with anterior cruciate ligament reconstruction: Combining knee joint computational modelling with follow-up T1ρ and T2 imaging," *Clin. Biomech.*, vol. 79, Oct. 2020, Art. no. 104844, doi: 10.1016/j.clinbiomech.2019.08.004.

[87] D. T. Felson *et al.*, "High prevalence of lateral knee osteoarthritis in Beijing Chinese compared with Framingham Caucasian subjects," *Arthritis Rheumatism*, vol. 46, no. 5, pp. 1217–1222, May 2002, doi: 10.1002/art.10293.

[88] I.-M. Lee and D. M. Buchner, "The importance of walking to public health," *Med. Sci. Sports Exercise*, vol. 40, no. 7, pp. S512–S518, 2008.

[89] J. L. Asay, A. Mündermann, and T. P. Andriacchi, "Adaptive patterns of movement during stair climbing in patients with knee osteoarthritis," *J. Orthopaedic Res.*, vol. 27, no. 3, pp. 325–329, Mar. 2009, doi: 10.1002/jor.20751.

[90] R. L. Mizner, S. C. Petterson, and L. Snyder-Mackler, "Quadriceps strength and the time course of functional recovery after total knee arthroplasty," *J. Orthopaedic Sports Phys. Therapy*, vol. 35, no. 7, pp. 424–436, Jul. 2005, doi: 10.2519/jospt.2005.35.7.424.

[91] D. Diracoglu, R. Aydin, A. Baskent, and A. Celik, "Effects of kinesthesia and balance exercises in knee osteoarthritis," *JCR, J. Clin. Rheumatol.*, vol. 11, no. 6, pp. 303–310, Dec. 2005, doi: 10.1097/01.rhu.0000191213.37853.3d.

[92] N. F. Bakker *et al.*, "A most painful knee does not induce interlimb differences in knee and hip moments during gait in patients with knee osteoarthritis," *Clin. Biomech.*, vol. 89, Oct. 2021, Art. no. 105455, doi: 10.1016/J.CLINBIOMECH.2021.105455.

[93] R. L. Mizner, S. C. Petterson, J. E. Stevens, M. J. Axe, and L. Snyder-Mackler, "Preoperative quadriceps strength predicts functional ability one year after total knee arthroplasty," *J. Rheumatol.*, vol. 32, no. 8, pp. 1533–1539, Aug. 2005.

[94] A. Rajagopal, C. L. Dembia, M. S. DeMers, D. D. Delp, J. L. Hicks, and S. L. Delp, "Full body musculoskeletal model for muscle-driven simulation of human gait," *IEEE Trans. Biomed. Eng.*, vol. 63, no. 10, p. 2068, Oct. 2016, doi: 10.1109/TBME.2016.2586891.

[95] J. P. Walter *et al.*, "Muscle synergies may improve optimization prediction of knee contact forces during walking," *J. Biomech. Eng.*, vol. 136, no. 2, Feb. 2014, Art. no. 021031, doi: 10.1115/1.4026428.

[96] L. P. Räsänen, "Three dimensional patient-specific collagen architecture modulates cartilage responses in the knee joint during gait," *Comput. Methods Biomech. Biomed. Eng.*, vol. 19, no. 11, pp. 1225–1240, Aug. 2016, doi: 10.1080/10255842.2015.1124269.

[97] M. S. Venäläinen *et al.*, "Quantitative evaluation of the mechanical risks caused by focal cartilage defects in the knee," *Sci. Rep.*, vol. 6, no. 1, p. 37538, Dec. 2016, doi: 10.1038/srep37538.

[98] D. J. Saxby *et al.*, "Machine learning methods to support personalized neuromusculoskeletal modelling," *Biomech. Model. Mechanobiol.*, vol. 19, no. 4, pp. 1169–1185, Aug. 2020, doi: 10.1007/s10237-020-01367-8.

[99] C. Pizzolato, M. Reggiani, D. J. Saxby, E. Ceseracciu, L. Modenese, and D. G. Lloyd, "Biofeedback for gait retraining based on real-time estimation of tibiofemoral joint contact forces," *IEEE Trans. Neural Syst. Rehabil. Eng.*, vol. 25, no. 9, pp. 1612–1621, Sep. 2017, doi: 10.1109/TNSRE.2017.2683488.

[100] G. A. Orozco *et al.*, "Shear strain and inflammation-induced fixed charge density loss in the knee joint cartilage following ACL injury and reconstruction: A computational study," *J. Orthopaedic Res.*, pp. 1–18, 2021, doi: 10.1002/jor.25177.